

Bound near-equatorial orbits around neutron stars

D. Marković [★]

Center for Theoretical Astrophysics, University of Illinois at Urbana-Champaign, 1110 West Green Street, Urbana, IL 61801, USA
 draza@qpo.physics.uiuc.edu

31 October 2018

ABSTRACT

Recent discovery of kilohertz quasi-periodic brightness oscillations of low mass X-ray binaries (LMXBs) has attracted attention to highly relativistic periodic motion near accreting neutron stars. Most models proposed so far involve (almost) inertial motion in the vicinity of the stars’ innermost stable circular orbits. In the present paper we study general-relativistic circular and eccentric orbits around spinning neutron stars assuming the orbits are slightly tilted with respect to the stars’ equatorial planes. We develop analytical and numerical techniques for integrating bound timelike geodesics in fully relativistic neutron star spacetimes obtained by modern numerical codes. We use equations of state of neutron star matter that span a broad range of stiffness, while the explored range of masses ($M > 1.7M_{\odot}$) and spin frequencies ($\nu_s < 600$ Hz) is motivated by the observations of LMXBs. We investigate the general-relativistic effects of periastron advance and nodal precession in the strong gravitational fields of rotating neutron stars and compare quantitatively the associated orbital frequencies with the more readily obtainable frequencies of orbits around Kerr black holes on the one hand, and low-order post-Newtonian (PN) expansions, on the other. While Kerr results approximate the periastron advance frequency much better than the PN expressions, the retrograde torque caused by the high quadrupole moments of the rotating stars clearly favours the PN approximation in the case of nodal precession. The methods developed in the present paper are used in the companion paper to test recent hypotheses regarding the origin of quasi-periodic oscillations in accreting neutron star sources.

Key words:

1 INTRODUCTION AND OVERVIEW

Over the past four years, observations by the Rossi XTE satellite of low-mass X-ray binaries (LMXBs) have produced an abundance of data on the rapid variations of these sources’ X-ray brightness (see van der Klis 1998, 2000, for an overview, and references therein). Most prominent in the sources’ high-resolution power spectra, the kilohertz-range quasi-periodic oscillations (QPOs) have been detected in ~ 20 binaries with compact accretors identified as neutron stars. The kHz QPOs often occur in pairs at frequencies ν_1 and $\nu_2 > \nu_1$ (with ν_2 ranging between 500 Hz and 1200 Hz) that can vary in a single source by up to a factor of ~ 2 (over as little as few minutes) in step with an inferred change in the accretion rate. In addition to the kHz QPOs, the horizontal-branch oscillations (HBOs) of the high-luminosity (near Eddington) neutron-star Z sources and ‘bumps’ in the power spectra of the lower-luminosity (between $10^{-3}L_{\text{Edd}}$ and a few $10^{-1}L_{\text{Edd}}$) atoll sources (for

the definition and properties of the Z and atoll sources see Hasinger & van der Klis 1989) have been observed at lower frequencies $10 \text{ Hz} \lesssim \nu_L \lesssim 60 \text{ Hz}$. These frequencies also vary in apparently tight correlation with the kHz QPO frequencies.

The fact that the kHz QPO frequencies lie in the range of orbital frequencies of bound geodesics near neutron-star-mass objects [the Kepler frequency for the innermost stable circular orbit (ISCO) around a static, spherical star of mass M is $\nu_{\text{ISCO}} = 1100 \text{ Hz} (2M_{\odot}/M)$] motivated several theoretical scenarios (see, e.g., Strohmayer *et al.* 1996, Miller, Lamb & Psaltis 1998, Stella & Vietri 1999) for the X-ray luminosity modulation that all involve inertial or near-inertial motion of localised condensations — variously named ‘clumps’ or ‘blobs’ — in the accretion flows around neutron stars. For instance, in a purely inertial (geodesic) orbital model, Stella & Vietri (1999; see also Karas 1999) have proposed for a given source an identification of the variable QPO frequencies ν_2 and ν_1 with, respectively, the Kepler frequencies ν_K and the periastron advance frequencies ν_{PA} of a family of eccentric orbits. The preferred plane of accretion (and, thus, of

[★] Also Department of Physics.

the clumps' motion) is normally assumed to lie close to the rotation equator of the central neutron star, a natural consequence of accretion-driven neutron star spin-up (similar reasoning clearly favours *prograde* motion in the accretion flow). However, we need not exclude *small* deviations of the orbits from the equatorial plane, and so it has been speculated that a signal — e.g., the QPOs observed at frequency ν_L — might be produced by the nodal precession of the orbital planes at frequency ν_{NP} or its first overtone (see, e.g., Stella & Vietri 1998 and Morsink & Stella 1999 for the nodal precession of circular orbits).

If any of the orbital models is confirmed, observation of orbital frequencies would provide a direct probe of the highly curved spacetimes around rapidly spinning neutron stars and an unprecedented test of the general theory of relativity in the strong-field regime. The highly accurate measurements of the kHz QPO frequencies (e.g., the relative error $\lesssim 1\%$ for Sco X-1; van der Klis *et al.* 1997) impose, however, stringent requirements on the QPO models; they also make it necessary to know the theoretical orbital frequencies with an accuracy that may render post-Newtonian approximations inadequate. Similarly, the spacetimes around neutron stars can differ from the Kerr black-hole spacetimes to such a degree as to invalidate the use of Kerr-based orbital frequencies.

It is our purpose in the present and a companion paper to investigate in some detail orbital motion near the equatorial planes of neutron stars and to test carefully the agreement between the frequencies of bound orbits with the QPO frequencies observed so far in neutron-star LMXBs. Specific QPO models will be compared with the existing data in the companion paper (Marković & Lamb 2000). In the present paper we study the motion of test particles on orbits of arbitrary eccentricity around rapidly spinning neutron stars. We pay particular attention to the general-relativistic effects of periastron advance and nodal precession in the neutron stars' strong gravitational fields, and compare quantitatively the orbital frequencies associated with these effects with the more readily obtainable frequencies of orbits around Kerr black holes on the one hand, and low-order post-Newtonian (PN) expansions, on the other. As the basis of our study, we set out to develop analytical and numerical techniques for a sufficiently accurate computation of the frequencies of orbits in fully general relativistic numerical neutron star spacetimes. Modern numerical codes (Komatsu, Eriguchi & Hachisu 1989a,b; Cook, Shapiro & Teukolsky 1992, 1994a,b; Stergioulas & Friedman 1995; Nozawa *et al.* 1998) allow an accurate computation of equilibrium uniformly spinning neutron star models starting from an arbitrary tabulated equation of state (EOS), and it is one variant (Stergioulas & Friedman 1995) that we use to obtain external neutron star spacetimes in which we then integrate the equations of motion for bound geodesics.

The numerical neutron star models discussed in this paper are all based on three equations of state that sample a broad range of stiffness, from the moderately stiff EOS C (Bethe & Johnson 1974; see also the early review by Arnett & Bowers, 1977) to the very stiff EOS L (Pandharipande & Smith 1975). The classic EOS C describes cold nucleon (n and p) + hyperon (λ , $\Sigma^{\pm,0}$, $\Delta^{\pm,0}$ and Δ^{++}) matter with the nucleon-nucleon potential represented by a set of Yukawa functions. The high-density behaviour is dominated

by the strong short-range repulsion due to the ω -meson exchange. EOS C allows the maximum mass of $1.86M_{\odot}$ for non-rotating stars. On the other hand, EOS L, based on coupling of (non-relativistic) nuclear matter to a mean scalar field, provides for a much higher maximum mass, $2.71M_{\odot}$, for non-rotating neutron stars and, accordingly, larger equatorial radii. For the third EOS of intermediate stiffness we choose EOS UU (Wiringa, Fiks & Fabrocini 1988), which, besides including the nucleon-nucleon potential (specifically, the Urbana v_{14}), achieves the relatively greater stiffness at high density due to the Urbana VII three-nucleon potential (Schiavilla, Pandharipande, & Wiringa 1986). The maximum non-rotating NS mass for this EOS is $2.20M_{\odot}$. [The more recent EOS A18+UIX + δv_b of Akmal, Pandharipande and Ravenhall (1998; see also Pandharipande, Akmal & Ravenhall, 1998) is based on the modern Argonne v_{18} two-nucleon potential and the Urbana IX three-nucleon potential and allows for the dependence of the interaction between two nucleons on their *total* centre-of-mass momentum; its stiffness is similar to that of EOS UU and the maximum non-rotating stellar mass is $2.23M_{\odot}$.] These three equations of state span the entire range of EOS stiffness that can provide the neutron star masses ($1.7 < M < 2.2$; from now on all masses will be given in units of solar mass) and radii required by the QPO models discussed in the companion paper (Marković & Lamb 2000).

In Section 2, we derive the equations of motion for a general bound geodesic near the equatorial plane of the stationary spacetime around a neutron star. The equations of motion involve the values of four radius-dependent potentials (provided as a tabulated output from a NS-model numerical code) in the equatorial plane, as well as the potentials' second derivatives with respect to the vertical coordinate. The presence of two integrals of motion, the energy E and the vertical component, L , of the angular momentum, allows integration of the radial and azimuthal equations up to quadratures (we specifically solve for *prograde* orbits). For orbits (slightly) tilted relative to the equatorial plane, the lack of a third integral of motion leaves one with two first-order Hamilton's equations for the vertical θ -motion. The precession of the orbital plane is then most conveniently analysed by means of Floquet's method. In the balance of Section 2 we discuss similar motion in the Kerr black hole spacetime, where the presence of a third integral of motion, the Carter constant, simplifies the treatment considerably. Finally, we briefly discuss low-order post-Newtonian expressions for the periastron advance and nodal precession frequencies.

In Section 3, we illustrate, by means of several examples, the salient features of the orbits around neutron stars, devoting most of our discussion to the dependence of the orbital frequencies, ν_K , $\nu_r = \nu_K - \nu_{\text{PA}}$ and ν_{NP} , on the radii of circular orbits or the periastra and apastron of eccentric orbits (unless specified otherwise, all radii will be given in units GM/c^2). We pay particular attention to the manner in which the frequency profiles are affected by equations of state of various stiffness. For instance, the stiffer EOS yield neutron stars of greater extent, which, in turn, can exclude highly eccentric orbits with small periastra and low ν_r . The larger stellar extent (and, accordingly, greater magnitude of the quadrupole moment qG^2M^3/c^4) also reduces significantly the nodal precession frequencies for stars of given

mass M and angular momentum jGM^2/c (this effect was previously explored for circular orbits by Morsink & Stella 1999). We also assess the accuracy of approximating the orbital frequencies in neutron-star spacetimes by the more readily computed frequencies of orbits in Kerr spacetimes of the same mass M and angular momentum jGM^2/c , or by the frequencies obtained from low-order post-Newtonian expressions (including the relatively large mass quadrupole terms characteristic of neutron stars). The results of this paper are summarised and discussed in Section 4.

Equipped with accurately computed frequencies of orbits in neutron star spacetimes, we proceed in the companion paper (Markovic & Lamb 2000) to investigate the possibility of their matching the QPO frequencies of neutron-star LMXBs.

2 BOUND GEODESICS AROUND SPINNING COMPACT STARS

2.1 Neutron stars

The code of Stergioulas (Stergioulas & Friedman 1995) yields the metric around a neutron star in the form isotropic in the $\bar{r} - \theta$ sector

$$ds^2 = -e^{\rho+\gamma} dt^2 + e^{\gamma-\rho} \bar{r}^2 \sin^2 \theta (d\phi - \omega dt)^2 + e^{2\alpha} (d\bar{r}^2 + \bar{r}^2 d\theta^2), \quad (1)$$

where $\gamma(\bar{r}, \theta)$, $\rho(\bar{r}, \theta)$, $\alpha(\bar{r}, \theta)$, $\omega(\bar{r}, \theta)$ are the four potentials computed numerically. The integration of orbital equations, described below, requires the four potentials to be given as smooth functions of \bar{r} . We achieve sufficient smoothness through a combination of spline and high-order Chebyshev polynomial representations (see, e.g., Press *et al.* 1992). Throughout the paper, r will denote only the coordinate-independent *circumferential* radius. For metric (1), $r = \exp[(\gamma - \rho)/2] \bar{r}$.

The metric components' independence of t and ϕ implies that the components $u_t \equiv -E$ and $u_\phi \equiv L$ of the 4-velocity of a test particle are conserved. It immediately follows that

$$\begin{aligned} \frac{dt}{d\tau} &= e^{-(\rho+\gamma)} (E - \omega L) \\ \frac{d\phi}{d\tau} &= \frac{L}{\bar{r}^2 \sin^2 \theta} e^{\rho-\gamma} + \omega e^{-(\rho+\gamma)} (E - \omega L). \end{aligned} \quad (2)$$

Assume for the moment a purely equatorial motion, $\theta = \pi/2$. The normalisation $u^\mu u_\mu = -1$ leads then to the equation for radial motion

$$\begin{aligned} \left(\frac{d\bar{r}}{d\tau} \right)^2 &= F(\bar{r}) \\ &\equiv e^{-2\alpha} \left[e^{-(\rho+\gamma)} (E - \omega L)^2 - \frac{L^2}{\bar{r}^2} e^{\rho-\gamma} - 1 \right]. \end{aligned} \quad (3)$$

For given apastron radius \bar{r}_a and periastron radius \bar{r}_p , a bound orbit exists if one can find L ($L > 0$ for prograde orbits) such that $F_a = F_p = 0$ (subscripts denote the values of \bar{r} at which the quantities are evaluated), i.e., such that solve the equations

$$E = \omega_a L + (A_a L^2 + B_a)^{1/2} = \omega_p L + (A_p L^2 + B_p)^{1/2}, \quad (4)$$

where $A(\bar{r}) \equiv \exp[2\rho(\bar{r})/\bar{r}^2]$ and $B(\bar{r}) = \exp[\rho(\bar{r}) + \gamma(\bar{r})]$.

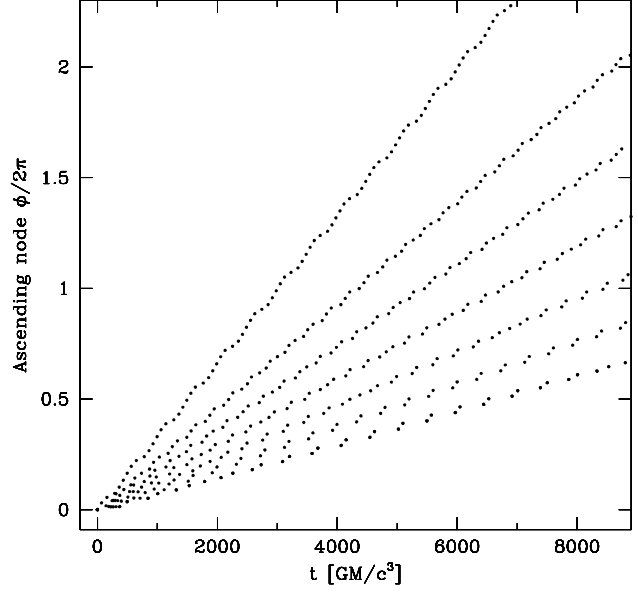


Figure 2. The drift of ascending nodal points for eccentric orbits of common periastron $r_p = 4.7$ (the same NS as in Fig. 1; throughout the paper r denotes the *circumferential* radius) and apastra $r_a = 8.0$ ($\nu_K = 1400$ Hz, $\nu_{\text{NP}} = 38$ Hz), 9.5 (1120, 26), 11.3 (964, 21), 13.4 (821, 17), 16.0 (692, 14), 19.2 (577, 11) and 23.0 (475, 8.6).

The required solution exists only if $\bar{r}_p > \bar{r}_{\text{mb}}$, where \bar{r}_{mb} is the periastron of the marginally bound ($E = 1$) orbit. Generally, for L and E corresponding to a bound orbit, there also is a third root of the equation $F(\bar{r}_3) = 0$, closer to the origin, $\bar{r}_3 < \bar{r}_p$. For the marginally bound orbit $\bar{r}_p = \bar{r}_3$, $\bar{r}_a = \infty$ [$F'(\bar{r}_p) = 0$, $F''(\bar{r}_p) > 0$; the prime denotes the derivative with respect to \bar{r}].

For a given $\bar{r}_p < \bar{r}_{\text{isco}}$, where \bar{r}_{isco} is the radius of the innermost stable circular orbit, there is a minimum apastron, $\bar{r}_{a,\text{min}}(\bar{r}_p) > \bar{r}_{\text{isco}}$ below which there exist no bound (prograde) orbits. For $\bar{r}_p > \bar{r}_{\text{isco}}$ we naturally have $\bar{r}_{a,\text{min}} = \bar{r}_p$.

Once L and E are found for given \bar{r}_p and \bar{r}_a , it is straightforward to obtain the period (in the distant observer's time t) of radial motion

$$\frac{1}{\nu_r} = 2 \int_{\bar{r}_p}^{\bar{r}_a} \frac{E - \omega L}{\sqrt{F}} e^{-(\rho+\gamma)} d\bar{r}, \quad (5)$$

as well as the frequency of azimuthal motion, i.e., the Kepler frequency

$$\nu_K = \frac{\Delta\phi}{\pi} \nu_r, \quad (6)$$

where

$$\begin{aligned} \Delta\phi &= \int_{\bar{r}_p}^{\bar{r}_a} \frac{\dot{\phi}}{\dot{\bar{r}}} d\bar{r} \\ &= \int_{\bar{r}_p}^{\bar{r}_a} \left[\frac{L}{\bar{r}^2} e^{\rho-\gamma} + \omega e^{-(\rho+\gamma)} (E - \omega L) \right] \frac{d\bar{r}}{\sqrt{F}}. \end{aligned} \quad (7)$$

The periastron advance frequency is then simply

$$\nu_{\text{PA}} = \nu_K - \nu_r. \quad (8)$$

In the more general case of orbits out of the equatorial plane, the motion is governed by the Hamiltonian (see, e.g.,

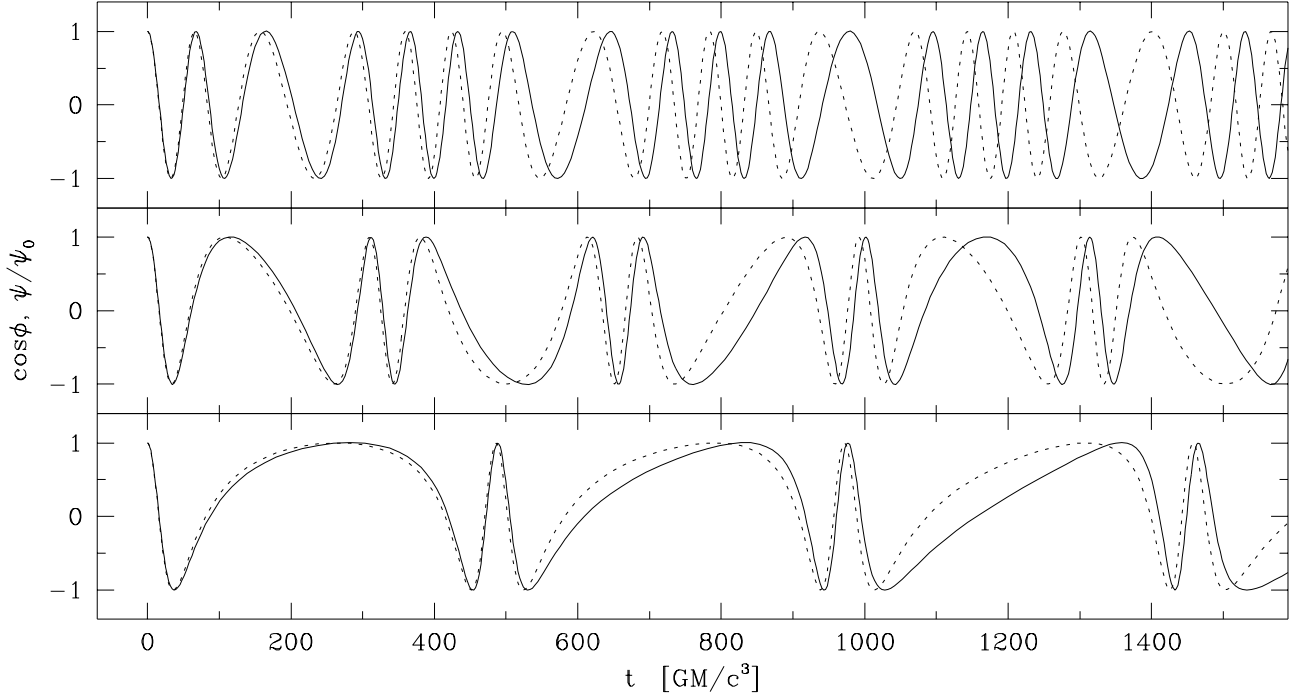


Figure 1. Plots of $\cos \phi$ (dotted lines) and ψ/ψ_0 (solid lines) for three eccentric orbits of common periastron $r_p = 4.7$ around a neutron star of mass $M = 1.8$, EOS UU, $\nu_s = 500$ Hz ($j = 0.20$). The apastra and the orbital frequencies are $r_a = 8.0$ ($\nu_K = 1400$ Hz, $\nu_{NP} = 38$ Hz), 13.4 (821, 17) and 23.0 (475, 8.6).

Misner, Thorne & Wheeler 1973)

$$H = -\frac{1}{2}e^{-(\rho+\gamma)}(E - \omega L)^2 + \frac{1}{2}e^{\rho-\gamma} \frac{L^2}{\bar{r}^2 \sin^2 \theta} + \frac{1}{2}e^{-2\alpha} \left(p_{\bar{r}}^2 + \frac{1}{\bar{r}^2} p_{\bar{\theta}}^2 \right). \quad (9)$$

For small displacements, $\psi \equiv \pi/2 - \theta$ ($p_{\psi} = -p_{\theta}$), from the equatorial plane, we can expand the four potentials, $\rho(\bar{r}, \psi) \approx \rho(\bar{r}, 0) + \bar{\rho}(\bar{r})\psi^2/2 \equiv \rho_0(\bar{r}) + \bar{\rho}(\bar{r})\psi^2/2$, etc., and thus arrive at the ‘harmonic oscillator’ form quadratic in both ψ and p_{ψ}

$$H = H_0(\bar{r}, p_{\bar{r}}) + \frac{1}{2}\Omega^2(\bar{r})\psi^2 + \frac{1}{2I(\bar{r})}p_{\psi}^2, \quad (10)$$

where

$$I(\bar{r}) \equiv e^{2\alpha_0} \bar{r}^2 \quad (11)$$

and

$$\Omega^2(\bar{r}) = e^{-(\rho_0+\gamma_0)} \left[(E - \omega_0 L)^2 \left(\frac{\bar{\rho}}{2} + \frac{\bar{\gamma}}{2} - \bar{\alpha} \right) + (E - \omega_0 L) L \bar{\omega} \right] + e^{\rho_0-\gamma_0} \frac{L^2}{\bar{r}^2} \left(1 + \frac{\bar{\rho}}{2} - \frac{\bar{\gamma}}{2} + \bar{\alpha} \right) + \bar{\alpha}. \quad (12)$$

Since the radial motion is (to the lowest order in ψ) given by equation (3) [and thus $H_0(\bar{r}, p_{\bar{r}}) = -1/2$], we have used this fact to substitute $p_{\bar{r}} = \exp(2\alpha_0) d\bar{r}/d\tau$ in the expression for $\Omega^2(\bar{r})$.

The motion in the ψ direction can now be computed

from Hamilton’s equations, given here in the matrix form,

$$\frac{d}{d\tau} \begin{pmatrix} \psi \\ p_{\psi} \end{pmatrix} = \mathbf{A} \begin{pmatrix} \psi \\ p_{\psi} \end{pmatrix}, \quad A_{12} = 1/I(\bar{r}), \quad A_{21} = -\Omega^2(\bar{r}), \quad A_{11} = A_{22} = 0, \quad (13)$$

where $\bar{r}(\tau)$ is a solution of equation (3).

The secular advance of the nodal line (i.e., the nodal precession) is a straightforward consequence of the failure of a particle to return to the initial ψ after a full revolution around the star. For example, in Fig. 1 we plot $\cos \phi$ and ψ/ψ_0 for three orbits of common periastron (circumferential) radius $r_p = 4.7$, which is smaller than $r_{\text{isco}} = 5.4$ for the neutron star of mass $M = 1.8$, EOS UU and spin frequency $\nu_s = 500$ Hz ($j = 0.20$). Notice the gradually increasing phase lag of the meridional motion relative to the azimuthal motion. This leads to a secular advance of the ascending node (see Fig. 2).

For eccentric orbits, the rate of the advance varies somewhat over a few orbital periods ν_K^{-1} : since the radial frequency ν_r is much smaller than ν_K for orbits close to r_{isco} (e.g., in the above example for $r_a = 8.0$, $\nu_r = 223$ Hz = $\nu_K/6.3$), a particle performs several revolutions (see the plot of $\cos \phi$ in Fig. 1) while lingering close to the periastron, and then moves closer to the apastron where both the rate of revolution and — in particular — the effects of the star’s spin and quadrupole deformation (oblateness) on the orbital motion are much weaker. However, when averaged over several orbital periods, the nodal precession rate is constant, and this *averaged* value is what we denote by ν_{NP} .

Equations (13) can be solved by direct integration over

a large number of (proper time) periods τ_r of radial motion to obtain the nodal drift with sufficient accuracy, as was done for Fig. 2. More economically, the same result can be obtained by Floquet's method (see, e.g., Arnol'd 1992 or Hochstadt 1975), as follows: We define the matrix

$$\Psi \equiv \begin{pmatrix} \psi_1 & \psi_2 \\ p_1 & p_2 \end{pmatrix}, \quad (14)$$

whose components are the values of the latitude ψ and the associated momenta p_ψ at the end of a period of radial motion, $\psi_1 \equiv \psi(\tau_r)$, $p_1 \equiv p_\psi(\tau_r)$ for initial conditions $\psi(0) = 1$, $p_\psi(0) = 0$, and $\psi_2 \equiv \psi(\tau_r)$, $p_2 \equiv p_\psi(\tau_r)$ for initial conditions $\psi(0) = 0$, $p_\psi(0) = 1$. Since the product of the eigenvalues of the matrix Ψ , $\mu_1\mu_2 = \exp\left(\int_0^{\tau_r} |\mathbf{A}| d\tau\right) = 1$, we obtain

$$\mu_1 = \mu_2^* = e^{i\nu_\psi/\nu_r}, \quad \cos(\nu_\psi/\nu_r) = \frac{\psi_1 + p_2}{2}, \quad (15)$$

where one must include (by an appropriate addition of $n2\pi$) the *total* phase change in ψ accumulated over τ_r when calculating ν_ψ/ν_r from equation (15). The nodal precession frequency ν_{PA} is then simply

$$\nu_{\text{NP}} = \nu_{\text{K}} - \nu_\psi. \quad (16)$$

The constants of motion L and E for almost equatorial *circular* orbits can be found at all $\bar{r} > \bar{r}_{\text{isco}}$ from the equations $F(\bar{r}) = F'(\bar{r}) = 0$. It is then straightforward to obtain the Kepler frequency [see equations (2)]

$$2\pi\nu_{\text{K}} = \frac{L}{(E - \omega L)\bar{r}^2} e^{2\rho} + \omega, \quad (17)$$

and the radial epicyclic frequency

$$2\pi\nu_r = \frac{[-F''(\bar{r})/2]^{1/2}}{E - \omega L} e^{\rho+\gamma}. \quad (18)$$

Using equations (11) and (13) we find the meridional frequency

$$2\pi\nu_\psi = \frac{\Omega(\bar{r})}{(E - \omega L)\bar{r}} e^{\gamma+\rho-\alpha}, \quad (19)$$

and thus the nodal precession frequency $\nu_{\text{NP}} = \nu_{\text{K}} - \nu_\psi$.

2.2 Kerr black holes

Expressed in the Boyer-Lindquist coordinates, the motion of a massive particle near the equatorial plane of a Kerr black hole is governed by the following equations (see, e.g., Chandrasekhar 1983)

$$\begin{aligned} \hat{r}^4 \dot{\hat{r}}^2 &= \mathcal{R}, \\ \hat{r}^4 \dot{\psi}^2 &= \Theta, \\ \hat{r}^2 \dot{\phi} &= \frac{1}{\Delta} [2jE\hat{r} + L(\hat{r}^2 - 2\hat{r})], \\ \hat{r}^2 \dot{t} &= \frac{1}{\Delta} [E\Sigma^2 - 2jL\hat{r}], \end{aligned} \quad (20)$$

where

$$\Delta \equiv \hat{r}^2 - 2\hat{r} + j^2, \quad \Sigma^2 \equiv (\hat{r}^2 + j^2)^2 - j^2\Delta \quad (21)$$

and

$$\begin{aligned} \mathcal{R}(\hat{r}) &= -(1 - E^2)\hat{r}^4 + 2\hat{r}^3 - [j^2(1 - E^2) + L^2]\hat{r}^2 \\ &\quad + 2(L - jE)^2\hat{r}, \end{aligned}$$

$$\Theta(\psi) = [L^2 + j^2(1 - E^2)](\psi_0^2 - \psi^2). \quad (22)$$

In the above equations we have set $\psi = 0$ everywhere except for the terms of order ψ^2 in the equation for the ψ -motion. The amplitude ψ_0 of the angular displacement ψ from the equatorial plane is related to the Carter constant.

For bound orbits ($E < 1$), the equation $\mathcal{R}(\hat{r}) = 0$ has three positive roots $\hat{r}_a > \hat{r}_p > \hat{r}_3$, and the first of equations (20) takes on the form

$$\hat{r}^3 \dot{\hat{r}}^2 = -(1 - E^2)(\hat{r} - \hat{r}_a)(\hat{r} - \hat{r}_p)(\hat{r} - \hat{r}_3). \quad (23)$$

Taking \hat{r}_a and \hat{r}_p as independent variables and defining $A \equiv \hat{r}_a + \hat{r}_p$ and $B \equiv \hat{r}_a\hat{r}_p$, we obtain from the coefficients of equation (23) the following relations

$$\begin{aligned} \frac{2}{1 - E^2} &= A + \hat{r}_3, \\ j^2 + \frac{L^2}{1 - E^2} &= B + A\hat{r}_3, \\ 2\frac{(L - jE)^2}{1 - E^2} &= B\hat{r}_3. \end{aligned} \quad (24)$$

Eliminating E and L from equations (24) we obtain a second-order equation for \hat{r}_3

$$D_2\hat{r}_3^2 + D_1\hat{r}_3 + D_0 = 0, \quad (25)$$

where

$$\begin{aligned} D_0 &= (2B - j^2A)^2 \\ D_1 &= 2(2B - j^2A)(2A - B - j^2) - 4j^2(A - 2)B \\ D_2 &= (2A - B - j^2)^2 - 4j^2B. \end{aligned} \quad (26)$$

Once \hat{r}_3 is found for given \hat{r}_p and \hat{r}_a , the angular momentum and energy are obtained straightforwardly

$$\begin{aligned} L^2 &= \frac{2}{\hat{r}_a + \hat{r}_p + \hat{r}_3} (\hat{r}_a\hat{r}_p + \hat{r}_p\hat{r}_3 + \hat{r}_3\hat{r}_a - j^2), \\ E^2 &= 1 - \frac{2}{\hat{r}_a + \hat{r}_p + \hat{r}_3}. \end{aligned} \quad (27)$$

Similarly to the neutron stars discussed above, for $\hat{r}_p > \hat{r}_{\text{mb}}$, where

$$\hat{r}_{\text{mb}} = 2 - j + 2\sqrt{1 - j} \quad (28)$$

is the Boyer-Lindquist periastron of the marginally bound ($E = 1$) prograde orbit, eccentric orbits exist only if $\hat{r}_a > \hat{r}_{a,\text{min}}$ where $\hat{r}_{a,\text{min}}(\hat{r}_p) > \hat{r}_{\text{isco}}$ and

$$\begin{aligned} \hat{r}_{\text{isco}} &= 3 + Z_2 - [(3 - Z_1)(3 + Z_1 + 2Z_2)]^{1/2}, \\ Z_1 &\equiv 1 + (1 - j^2)^{1/3} [(1 + j)^{1/3} + (1 - j)^{1/3}], \\ Z_2 &\equiv (3j^2 + Z_1^2)^{1/2}, \end{aligned} \quad (29)$$

is the radius of the innermost stable circular orbit. Again, $\hat{r}_{a,\text{min}} = \hat{r}_p$ if $\hat{r}_p > \hat{r}_{\text{isco}}$.

The two positive roots (if they exist, i.e., if there are bound orbits with the given apastron \hat{r}_a and periastron \hat{r}_p) of equation (25) correspond to prograde and retrograde orbits. Restricting ourselves for the moment to weakly bound orbits at large radii

$$\hat{r}_a, \hat{r}_p \gg 1; \quad 1 + E \approx 2, \quad U \equiv 1 - E \ll 1, \quad (30)$$

around almost spherical, $j \ll 1$, black holes, we obtain from equations (26)

$$\hat{r}_3 \simeq 2 \frac{B - j(A - 1)L}{B - 2A + 2jL}. \quad (31)$$

We see that $\hat{r}_3(L > 0) < \hat{r}_3(L < 0)$ and that the prograde orbits are more tightly bound than the retrograde ones, $U(L > 0) > U(L < 0)$. The prograde orbit thus corresponds to the smaller of the roots of equation (25).

The period of the radial motion is

$$\begin{aligned} \frac{1}{\nu_r} &= 2 \int_{\hat{r}_p}^{\hat{r}_a} \frac{\dot{t}}{\hat{r}} d\hat{r} \\ &= 2 \int_0^\pi \frac{E\Sigma^2 - 2jL\hat{r}}{\Delta\sqrt{\hat{r}(1-E^2)(\hat{r}-\hat{r}_3)}} d\chi, \end{aligned} \quad (32)$$

where we have introduced a convenient integration parameter χ such that

$$\hat{r} = \hat{l}(1 + \epsilon \cos \chi), \quad \hat{l} \equiv \frac{\hat{r}_a + \hat{r}_p}{2}, \quad \epsilon \equiv \frac{\hat{r}_a - \hat{r}_p}{\hat{r}_a + \hat{r}_p}. \quad (33)$$

Using the general relation (6) to find the Kepler frequency, we integrate the third of equations (20) and thus obtain

$$\begin{aligned} \Delta\phi &= \int_{\hat{r}_p}^{\hat{r}_a} \frac{\dot{\phi}}{\hat{r}} d\hat{r} \\ &= \int_0^\pi \frac{2jE\hat{r} + L(\hat{r}^2 - 2\hat{r})}{\Delta\sqrt{\hat{r}(1-E^2)(\hat{r}-\hat{r}_3)}} d\chi. \end{aligned} \quad (34)$$

Finally, the second of equations (20) and the second of equations (22) give the motion in the ψ -direction

$$\psi = \psi_0 \cos \left(\sqrt{L^2 + j^2(1-E^2)} \int_{\hat{r}}^{\hat{r}_a} \frac{1}{\hat{r}} \frac{1}{\hat{r}^2} d\hat{r} \right). \quad (35)$$

The failure of a particle to return to the initial ψ after a full period of azimuthal motion will lead to a secular precession of the orbital plane (i.e., the nodal precession) at frequency (16) where

$$\begin{aligned} \nu_\psi &= \nu_r \frac{1}{\pi} \sqrt{L^2 + j^2(1-E^2)} \int_{\hat{r}_p}^{\hat{r}_a} \frac{1}{\hat{r}} \frac{1}{\hat{r}^2} d\hat{r} \\ &= \nu_r \frac{1}{\pi} \sqrt{L^2 + j^2(1-E^2)} \\ &\quad \times \int_0^\pi \frac{1}{\sqrt{\hat{r}^5(1-E^2)(\hat{r}-\hat{r}_3)}} d\chi. \end{aligned} \quad (36)$$

For a circular orbit at Boyer-Lindquist radius \hat{r} near the equatorial plane, the Kepler frequency for prograde orbits is (see, e.g., Chandrasekhar 1983)

$$2\pi\nu_K = \frac{1}{\hat{r}^{3/2}(1+j\hat{r}^{-3/2})} \quad (37)$$

(to obtain expressions for retrograde orbits one should set $j \rightarrow -j$). At all $\hat{r} > \hat{r}_{\text{isco}}$ a slight perturbation of the orbital motion in the radial direction will lead to radial oscillations at the radial epicyclic frequency

$$\nu_r = |\nu_K| (1 - 6\hat{r}^{-1} + 8j\hat{r}^{-3/2} - 3j^2\hat{r}^{-2})^{1/2}. \quad (38)$$

On the other hand, a particle in a circular orbit tilted slightly with respect to the equatorial plane will undergo meridional oscillations at frequency

$$\nu_\psi = |\nu_K| (1 - 4j\hat{r}^{-3/2} + 3j^2\hat{r}^{-2})^{1/2} \quad (39)$$

leading to the nodal precession at frequency (16).

At large radii ($r \gtrsim 10$), the asymptotic expressions $2\pi\nu_{\text{PA}} \approx 3\hat{r}^{-5/2}$ and $2\pi\nu_{\text{NP}} \approx 2j\hat{r}^{-3}$ lead to the simple scaling

$$\nu_{\text{NP}} \approx j\pi^{1/5} \left(\frac{2}{3}\right)^{6/5} \nu_{\text{PA}}^{6/5}. \quad (40)$$

At smaller radii, the slope $d \ln \nu_{\text{NP}} / d \ln \nu_{\text{PA}}$ steadily decreases with increasing frequencies and drops below unity near the innermost stable circular orbit.

2.3 Spinning stars in post-Newtonian approximation

At a sufficiently large distance from a spinning star of angular momentum jGM^2/c and quadrupole moment qG^2M^3/c^4 ($q < 0$ for oblate bodies) we can use post-Newtonian (PN) expansions (see, e.g., Weinberg 1972) to obtain approximate expressions for the periastron advance and nodal precession frequencies. Thus, for a nearly equatorial orbit of semilatus rectum $l \equiv 2r_a r_p / (r_a - r_p)$, eccentricity $\epsilon \equiv (r_a - r_p) / (r_a + r_p)$, and the Newtonian and post-Newtonian orbital (Kepler) frequencies

$$\begin{aligned} \nu_{\text{K,N}} &= \frac{1}{2\pi} \left(\frac{1 - \epsilon^2}{l} \right)^{3/2}, \\ \nu_{\text{K}} &= \nu_{\text{K,N}} \left[1 - (1 - 3\epsilon^2) \frac{1}{l} + \mathcal{O} \left(\frac{1}{l^{3/2}} \right) \right], \end{aligned} \quad (41)$$

the rate of periastron advance is

$$\begin{aligned} \nu_{\text{PA}} &= \nu_{\text{K}} \left[3 \frac{1}{l} + \frac{9}{2} \left(1 + \frac{\epsilon}{6} \right) \frac{1}{l^2} \right. \\ &\quad \left. - 4j \frac{1}{l^{3/2}} - \frac{3q}{2} \frac{1}{l^2} + \mathcal{O} \left(\frac{1}{l^{5/2}} \right) \right], \end{aligned} \quad (42)$$

where $\mathcal{O} \left(\frac{1}{l^{5/2}} \right)$ indicates terms of asymptotic order at least as high as $l^{-5/2}$. In equation (42), the first two terms are the 1st and 2nd PN corrections present even for a spherical star, the third term is due to the gravitomagnetic force, while the fourth term is the (Newtonian) effect of the star's rotation-induced deformation.

In the lowest-order PN approximation, the precession of the plane of an orbit around the star's spin axis is interpreted as being caused by the gravitomagnetic force. Together with the purely Newtonian quadrupole precession, the nodal precession rate is

$$\nu_{\text{NP}} = \nu_{\text{K}} \left[2j \frac{1}{l^{3/2}} + \frac{3q}{2} \frac{1}{l^2} + \mathcal{O} \left(\frac{1}{l^{5/2}} \right) \right]. \quad (43)$$

While for a Kerr black hole $q = -j^2$ [cf. equations (37) and (39)], the ratio $-q/j^2$ is considerably larger for neutron stars (Laarakkers & Poisson 1998); it ranges from ~ 2 to more than 10, depending on the mass and the equation of state.

3 BOUND ORBITS AROUND NEUTRON STARS: COMPARISON WITH KERR BLACK HOLE ORBITS

Equations of state of different stiffness give rise to a wide range of magnitude of the model neutron stars' rotation-induced deformation, and, consequently, significant differences in the spacetime geometries around them. It is our

	C		UU		L	
	R_e (km)	r_{isco} (km)	R_e (km)	r_{isco} (km)	R_e (km)	r_{isco} (km)
$j = 0.1$	4.08 (10.8)	5.69 (15.1)	4.13 (11.0)	5.69 (15.1)	5.69 (15.1)	5.72 (15.2)
$j = 0.2$	4.17 (11.1)	5.41 (14.4)	4.19 (11.1)	5.42 (14.4)	5.76 (15.3)	--- ---
	ν_s	q	ν_s	q	ν_s	q
$j = 0.1$	271	-0.024	249	-0.026	148	-0.056
$j = 0.2$	525	-0.090	490	-0.099	292	-0.209

Table 1. Stellar equatorial (circumference) radii R_e , ISCO radii, spin frequencies ν_s [Hz] and quadrupole moments q in units $G^2 M^3 / c^4$ for NS models of mass $M = 1.8$ and indicated angular momenta j . The radii are given both in units GM/c^2 and in kilometres.

main purpose in this Section to describe and quantify how the differing geometries imprint themselves on the potentially measurable frequencies of bound orbits around the stars, and to compare these frequencies with those of orbits around spinning (Kerr) black holes.

For neutron star models of given mass M and angular momentum jGM^2/c , the very stiff equations of state (e.g., EOS L as opposed to the ‘softer’ UU or yet ‘softer’ C) yield more extended neutron star models that undergo greater centrifugal deformation. This leads to higher mass quadrupole moments $qG^2 M^3 / c^4$ while requiring lower spin frequencies ν_s , as can be seen in Table 1.

As Laarakkers & Poisson (1998, LP) have shown, the magnitude of q grows nearly quadratically, $q \simeq -a(\text{EOS}, M)j^2$, over a broad range of j . While the constant a is much smaller for EOS C ($a \simeq 2.4$ for $j \lesssim 0.2$; LP compute $a \simeq 2.7$ for a much greater range of j) or EOS UU ($a \simeq 2.6$) than for the stiff EOS L ($a \simeq 5.2$; LP find $a \simeq 4.9$), it still exceeds by a large amount the (exact) value $a = 1$ for the Kerr black hole.

Based on the low-order PN expressions (42) and (43), one would expect a general trend toward higher ν_{PA} (i.e., lower ν_r) and lower ν_{NP} at given r (all radii used in this section are the coordinate-independent *circumferential* radii) as $-q$ is increased. This expectation is indeed borne out by our computation of circular orbital frequencies as can be seen, e.g., in Fig. 3 for a $M = 1.8$ family of NS models and black holes. Of course, a PN expansion cannot account for the strong-field relativistic effect of the vanishing of the radial epicyclic frequency at the radius r_{isco} of the innermost stable circular orbit; the large magnitude of q for a stiff EOS simply causes a faster drop of ν_r as r is reduced past the point of maximum ν_r . Quite generally, r_{isco} moves inward for higher j , an effect familiar from the case of the Kerr spacetime (29).

The vertical bars in Fig. 3 mark the ranges of the maximal values of ν_r (the top panel) and ν_{NP} (the middle panel) for the indicated values of j . For each j we plot the frequencies for the three EOS, C, UU and L (all solid lines), and the Kerr black hole (the dotted line) of the same M and j . In all cases the curves for EOS C and UU almost coincide.

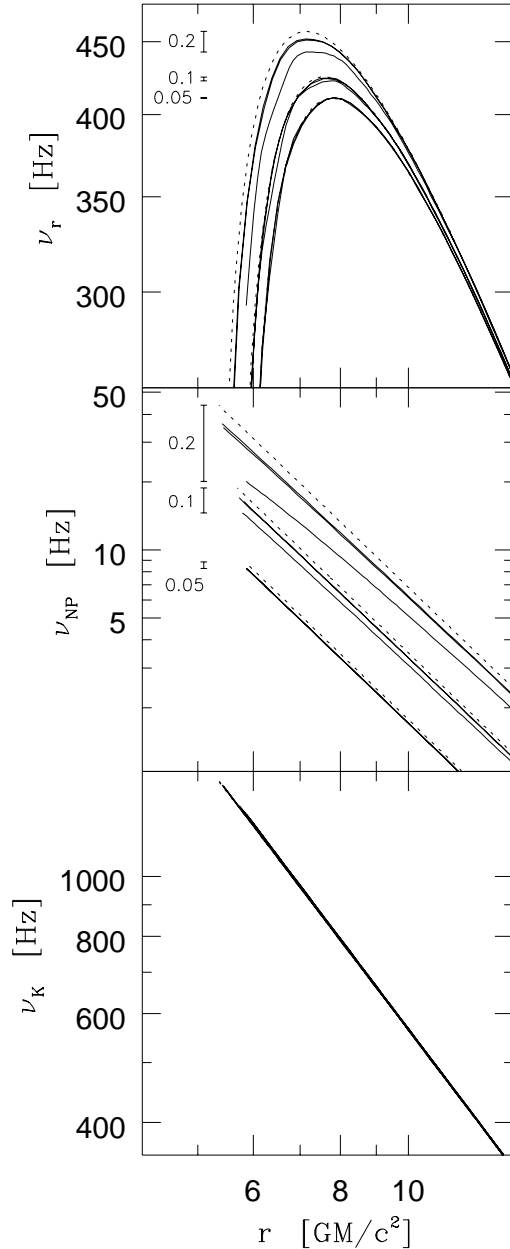


Figure 3. The radial, nodal precession, and Kepler frequencies as functions of the circumference radius for *circular* orbits around a $M = 1.8$ neutron stars (solid lines; EOS C, UU, and L) and Kerr black holes (dotted lines). The values of the angular momentum parameter j are indicated by the labels of vertical bars.

Whereas the drop in ν_r at $r < 10$ due to the star’s spin-induced deformation is relatively modest [$|\Delta\nu_r|/\nu_r \lesssim 15\%$; notice, however the considerable numerical error in ν_r for the stiff EOS L, due to the necessity of computing the second derivative (18) from the tabulated metric], the reduction in $\nu_{\text{NP}}(r)$ relative to the Kerr values is more pronounced, amounting at $j = 0.2$ to up to $\sim 20\%$ for EOS UU or even $\sim 40\%$ for EOS L. For lower j ($j < 0.1$), the difference between the frequencies for different EOS is less pronounced, and it virtually disappears at $j \sim 0.05$.

Of the three EOS, the stiff EOS L makes the star at $j = 0.2$ so extended at the equator, $R_e = 5.8GM/c^2 =$

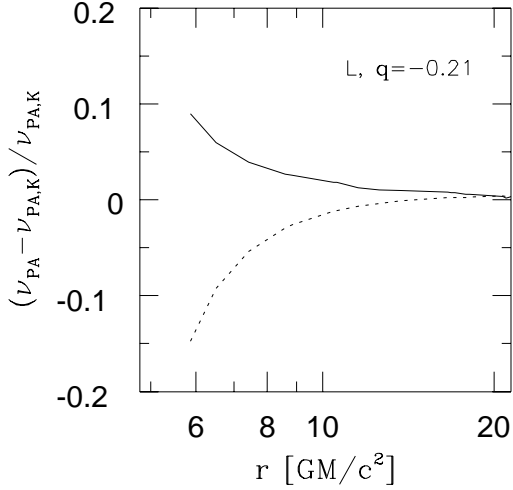


Figure 4. Relative deviation, $(\nu_{\text{PA}} - \nu_{\text{PA,K}})/\nu_{\text{PA,K}}$, with respect to the Kerr values (for the same M and j) of the periastron advance frequencies (solid line) and the post-Newtonian values (dotted line; see equation 42) for circular orbits around an $M = 1.8$, $j = 0.2$, EOS L ($q = -0.21$) neutron star.

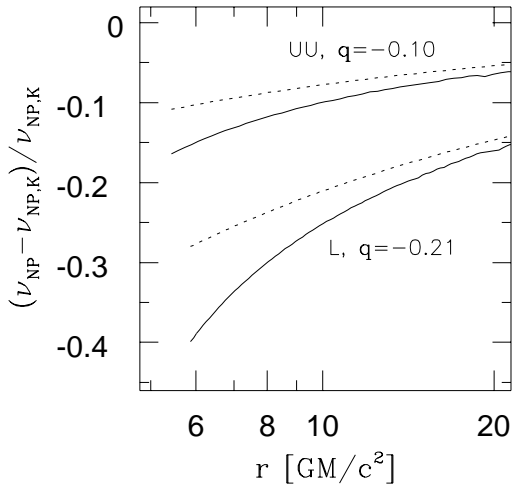


Figure 5. Relative deviations, $(\nu_{\text{NP}} - \nu_{\text{NP,K}})/\nu_{\text{NP,K}}$, with respect to the Kerr values (for the same M and j) of the nodal precession frequencies (solid lines) and the post-Newtonian values (dotted lines) for circular orbits around $M = 1.8$, $j = 0.2$ neutron stars. The EOS used are UU (yielding $q = -0.10$) for the upper solid line, and L ($q = -0.21$) for the lower solid line. The post-Newtonian values are obtained from equation (43) using the values of M , j and q of the corresponding neutron star models.

15.4 km, that there is no innermost stable circular orbit (see Table 1); the corresponding curve $\nu_r(r)$ thus never reaches the terminal point $\nu_r = 0$, in contrast with all the other cases shown in Fig. 3.

The simple low-order PN expressions (42) for ν_{PA} and (43) for ν_{NP} approximate rather accurately the actual frequencies of circular orbits of radii $r \gtrsim 10$, as can be seen from Figs. 4 and 5. As pointed out above, close to r_{isco} (i.e., for $r \lesssim 8$), the growth of the post-Newtonian ν_{PA} with decreasing r cannot model accurately the much faster growth of the relativistic ν_{PA} as it approaches ν_{K} . In this range, the Kerr

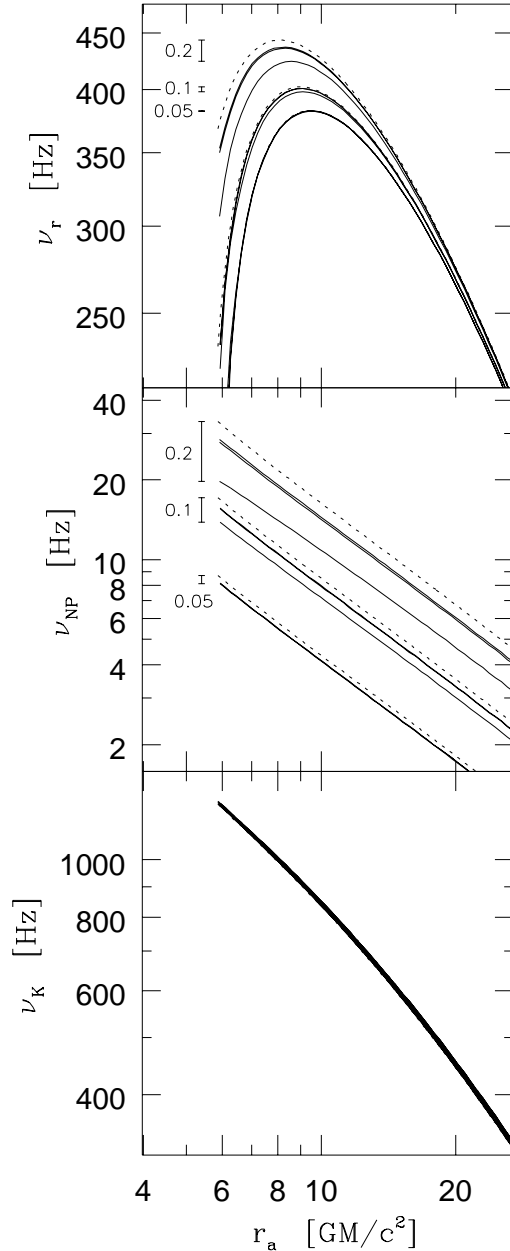


Figure 6. The radial, nodal precession and Kepler frequencies as functions of the apastron radius for eccentric orbits of common periastron $r_p = 5.88$ around $M = 1.8$ neutron stars (solid lines; EOS C, UU and L) and Kerr black holes (dotted lines). The values of the angular momentum parameter j are indicated by the labels of the vertical bars.

values for the same M and j furnish a considerably better approximation, as is evident in Fig. 4.

For the nodal precession, on the other hand, the large quadrupole term makes at all r the low-order expansion (43) a much better approximation than the Kerr $\nu_{\text{NP}}(r)$ (see Fig. 5). Notice, however, that for stiff EOS and for $r \lesssim 8$ (the lower curves of Fig. 5) the expansion (43) significantly overestimates the actual ν_{NP} which is, e.g., at the surface of the star, less than 60% of the corresponding Kerr value.

Turning now to eccentric orbits, one can distinguish between two broad classes, characterised by periastra r_p that

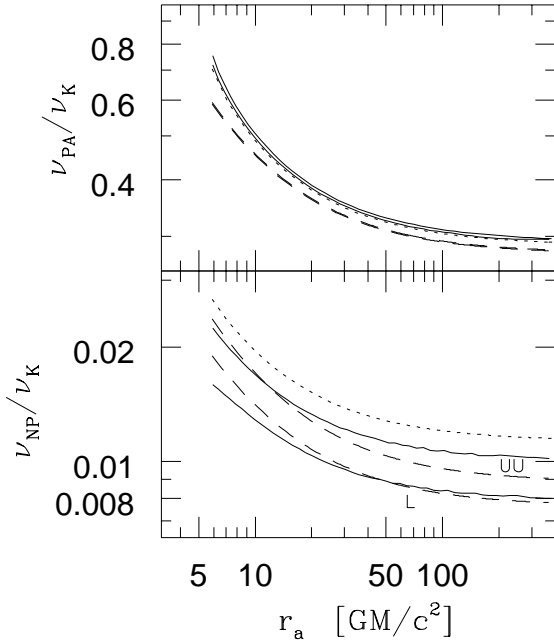


Figure 7. Ratios of orbital frequencies for $M = 1.8$, $j = 0.2$ and $r_p = 5.88$ for EOS L and UU (solid lines) and for the Kerr black hole (dotted lines) of the same M and j . PN values for $q = -0.21$ (EOS L) and $q = -0.10$ (EOS UU) are given by dashed lines.

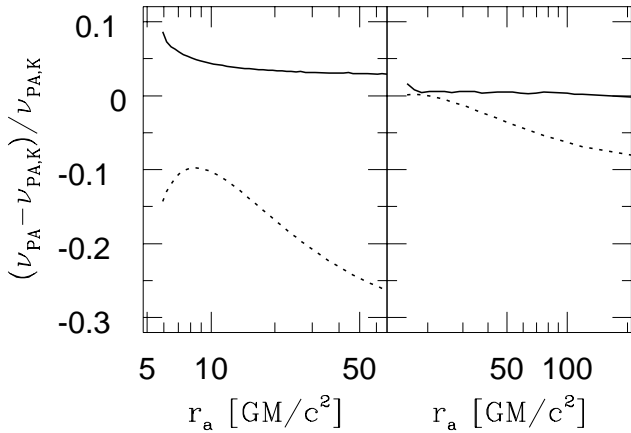


Figure 8. Relative deviations, $(\nu_{\text{PA}} - \nu_{\text{PA,K}})/\nu_{\text{PA,K}}$, with respect to the Kerr values (for the same M and j) of the periastron advance frequencies (solid lines) and the post-Newtonian values (dotted lines; see equation 42) for eccentric orbits around an $M = 1.8$, $j = 0.2$, EOS L ($q = -0.21$) neutron star. *Left panel:* eccentric orbits of common periastron $r_p = 5.88$. *Right panel:* eccentric orbits of common periastron $r_p = 15.0$.

are either larger or smaller than r_{isco} . Within the first class, $r_p > r_{\text{isco}}$ (so that $r_{\text{a,min}} = r_p$), the plots of the orbital frequencies as functions of r_a for a family of orbits of common periastron r_p resemble (an example is shown in Fig. 6) the frequency vs. radius plots for circular orbits shown above in Fig. 3. The obvious difference is that the magnitudes of the negative slopes $d\nu/dr_a$ are smaller than those of the slopes $d\nu/dr$ for circular orbits: even if r_a is large, the eccentric or-

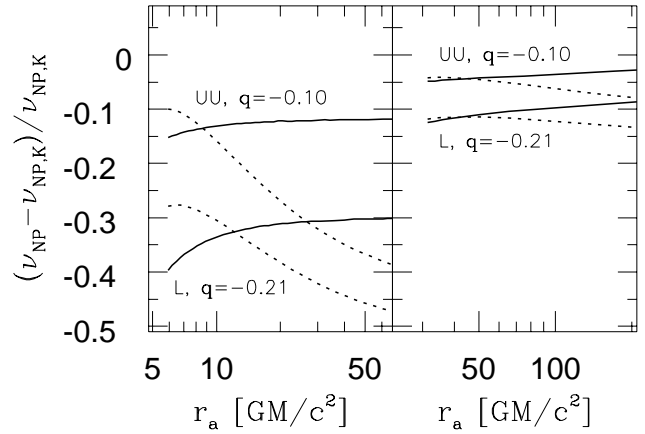


Figure 9. Relative deviations, $(\nu_{\text{NP}} - \nu_{\text{NP,K}})/\nu_{\text{NP,K}}$, with respect to the Kerr values (for the same M and j) of the nodal precession frequencies (solid lines) and the post-Newtonian values (dotted lines; see equation 43) for eccentric orbits around $M = 1.8$, $j = 0.2$ neutron stars. The EOS used are UU (yielding $q = -0.10$) for the upper solid and dotted lines, and L ($q = -0.21$) for the lower lines. *Left panel:* eccentric orbits of common periastron $r_p = 5.88$. *Right panel:* eccentric orbits of common periastron $r_p = 30.0$.

bits have access to small radii where relativistic effects, like frame dragging, take place. This can be seen from the PN expansions (42) and (43), in which the effect of increased periastron radius is ‘buffered’ by r_a ’s appearing in the expressions only through l , where $l \sim 2r_p$ for $r_a \gg r_p$ [the dependence on ϵ in (42) is weak]. For large r_a we therefore expect the ratios $\nu_{\text{PA}}/\nu_{\text{K}}$ and $\nu_{\text{NP}}/\nu_{\text{K}}$ to asymptote to constant values, as indeed is the case (see Fig. 7).

Although the PN expressions (42) and (43) reproduce qualitatively the profiles $\nu_{\text{PA}}(r_a)$ and $\nu_{\text{NP}}(r_a)$ obtained numerically from NS models, they tend to give a somewhat steeper fall-off at large r_a , thus falling short of the ‘exact’ values by up to $\sim 30\%$. This is evident in Fig. 7 and is displayed in greater detail in Figs. 8 and 9. It is a consequence of the extreme slowness of relativistic radial motion in the strong-field vicinity of r_{isco} : since relativistic effects (e.g., frame dragging) weaken rapidly at larger radii, this gives them more time to build up and the integrated effects thus exceed the PN estimates.

As in the case of circular orbits, the periastron advance frequency $\nu_{\text{PA}}(r_a)$ is modeled much better for all r_a by the Kerr black hole values (for the same M and j ; see Fig. 8) than by the PN expansion (42). As can be seen in the right panel of Fig. 8, only for $r_p > 10$ does the PN $\nu_{\text{PA}}(r_a)$ approach closely the values obtained from the numerically computed NS spacetimes.

Regarding the nodal precession, for moderately eccentric orbits, $r_a \lesssim 2r_p$, the PN expansion (43) is superior to the Kerr values at modeling $\nu_{\text{NP}}(r_a)$ obtained from the numerical NS spacetimes (see Fig. 9). The better accuracy of the PN frequencies is more prominent for stiff EOS, in a straightforward extension of the trend we observed for circular orbits. Again, for larger eccentricities, the numerical spacetimes’ $\nu_{\text{NP}}(r_a)$ inevitably split off from the PN curves and shift toward the Kerr values. As we increase r_p , the

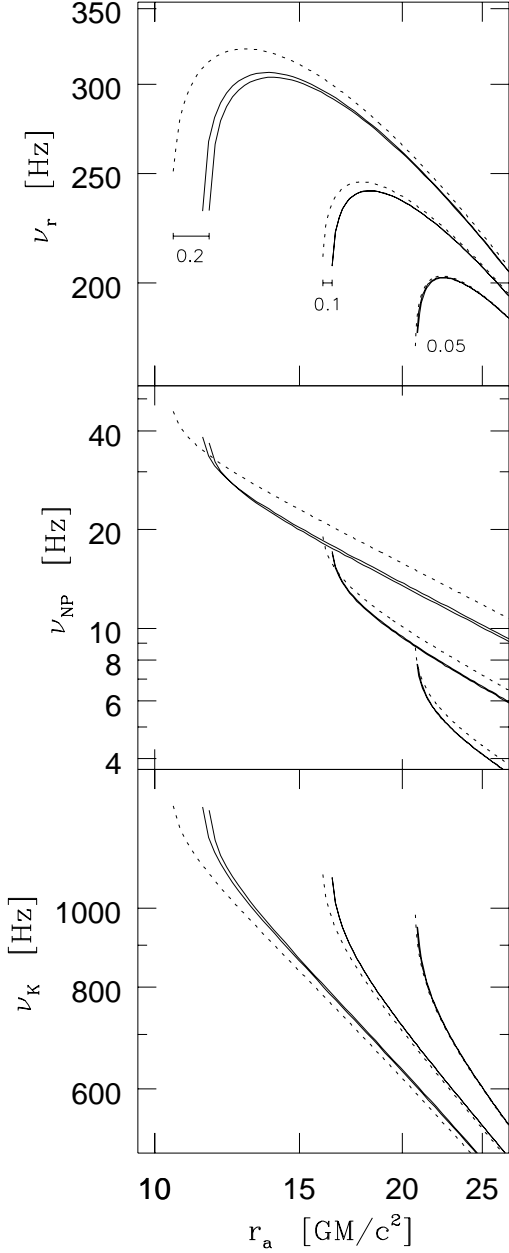


Figure 10. The radial, nodal precession and Kepler frequencies as functions of apastron radii of highly eccentric orbits of common periastron $r_p = 4.30$ around $M = 1.8$ neutron stars (solid lines; EOS C and UU) and Kerr black holes (dotted lines). The values of the angular momentum parameter j are indicated in the top panel.

range of eccentricity ϵ over which the PN expansion is relatively accurate increases; compare the two panels of Fig. 9.

For the second class of eccentric orbits with $r_p < r_{\text{isco}}$, we observe (see Fig. 10 for EOS C and UU) that at constant r_p the minimum apastron radius, $r_{a,\text{min}}(r_p)$, shrinks rapidly with increasing j , following the related reduction of r_{isco} (for both EOS, $r_{\text{isco}} = 5.84, 5.69$ and 5.42 for $j = 0.05, 0.1$ and 0.2 , respectively). Compared with the Kerr black hole, the main effect of the larger quadrupole moment of the NS is a larger $r_{a,\text{min}}(r_p)$ at given M and j as well as lower $\nu_r(r_a)$ and higher $\nu_{\text{PA}}(r_a)$. Notice, however, that as r_a approaches $r_{a,\text{min}}$

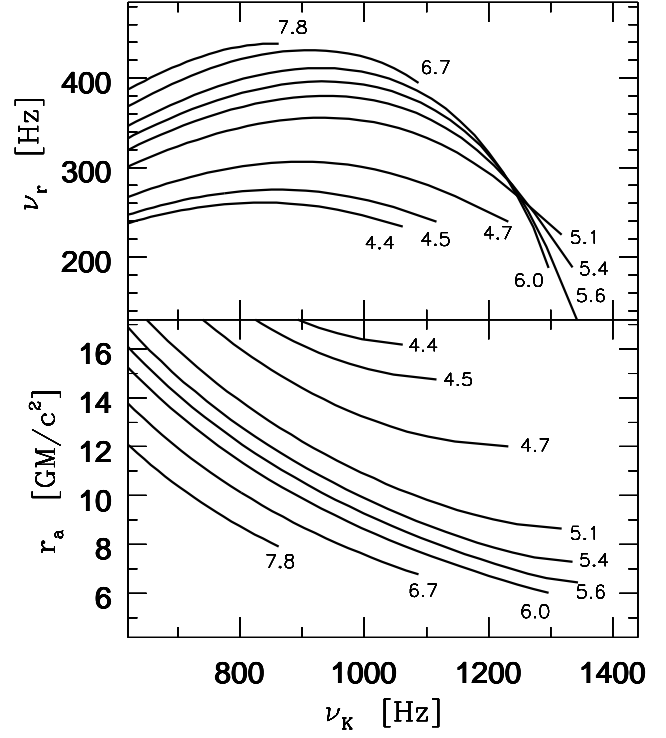


Figure 11. EOS UU: frequencies and apastra as functions of ν_K for families of eccentric orbits around a NS of $M = 1.7$ and $\nu_s = 100$ Hz ($R_e = 4.39 = 11.0$ km, $r_{\text{isco}} = 5.87 = 14.7$ km). The curves are labeled by the values of periastron in units GM/c^2 .

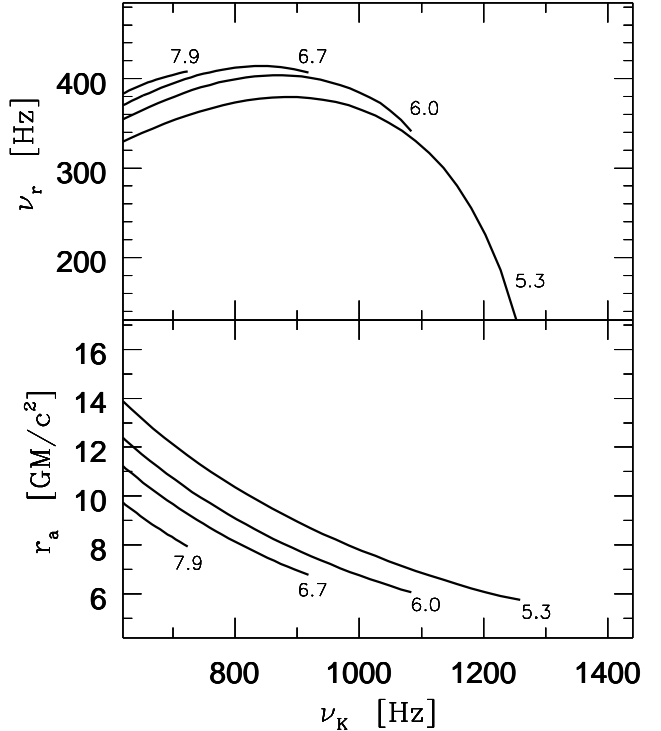


Figure 12. EOS L: frequencies and apastra for families of eccentric orbits around a NS of $M = 2$ and $\nu_s = 363$ Hz ($R_e = 5.23 = 15.4$ km, $r_{\text{isco}} = 5.44 = 16.1$ km).

from above, the functions $\nu_K(r_a)$ and $\nu_{\text{NP}}(r_a)$ bend upward abruptly, while $\nu_r(r_a)$ drops until it reaches the ‘terminal’ value $\nu_r(r_{a,\text{min}})$.

The sharp change of ν_K near $r_{a,\text{min}}$ leads to a ‘flat’ dependence $\nu_r(\nu_K)$ for a family of orbits of a given $r_p < r_{\text{isco}}$; see Fig. 11 for a relatively slow spinning, $\nu_s = 100$ Hz, EOS UU neutron star. As r_p is increased, the functions $\nu_r(\nu_K)$ at first grow steeper, with increasingly negative slopes at large ν_K (small r_a), until at $r_p = r_{\text{isco}}$, ν_r drops to zero for $\nu_K = \nu_{\text{isco}}$. A further growth of r_p again brings about flatter functions $\nu_r(\nu_K)$ but at considerably larger ν_r .

In Fig. 12 we show the functions $\nu_r(\nu_K)$ for eccentric orbits around a $M = 2$, $\nu_s = 363$ Hz, EOS L neutron star. The stiff equation of state makes the star large ($R_c = 5.3 = 15.6$ km) so that very low r_p orbits do not exist and the flat, low ν_r curves $\nu_r(\nu_K)$ seen in Fig. 11 are absent from Fig. 12. (This is why the plots of frequencies for the low $r_p = 4.3$ families of orbits in Fig. 10 could be shown only for the *moderately* stiff EOS C and UU.) As a consequence, the set of frequencies of eccentric orbits (for given M and ν_s) is a much more limited subset of the 2-dimensional ν_K - ν_r plane for the stiff EOS L than for the softer equations of state.

4 CONCLUSIONS

If shown to indeed be a manifestation of the orbital motion around neutron stars, the quasi-periodic oscillations of the low mass X-ray binaries would furnish an unprecedented probe of the strongly curved spacetime near the compact objects and allow inference of their masses M and spin rates ν_s . In particular, highly eccentric orbits, which near their periastra penetrate deeper than the innermost stable circular orbit, would put tight constraints on the sizes of neutron stars, and thus on the equation of state.

The high accuracy (e.g., better than $\sim 1\%$ for Sco X-1), with which the frequencies of the kHz QPO frequencies have been measured, makes it important to use the values obtained by integrating test-particle motion in fully relativistic numerical spacetimes that can be computed by spinning neutron star codes. For $j > 0.1$, and especially for orbits of considerable eccentricity, the post-Newtonian (PN) expansions or approximation with Kerr metric orbital frequencies are not sufficiently accurate.

In the case of the periastron advance frequency ν_{PA} , the Kerr results provide a better approximation to actual motion in the neutron star spacetimes than do the low-order PN expressions. Although the Kerr $\nu_{\text{PA,K}}$ is always lower than the value ν_{PA} for the same periastron and apastron (circumferential) radii in a neutron-star spacetime, it never falls below ν_{PA} by more than 10%, even for the highest angular momenta investigated here ($j \approx 0.2$) and for the stiffest EOS (L). The general-relativistic decrease of ν_r in the vicinity of the innermost stable orbit (ISCO) makes the PN approximations for ν_{PA} inaccurate even for moderately ($r_a/r_p \lesssim 2$) eccentric orbits if $r_p < 7$ (for highly eccentric orbits, PN is typically a poor approximation).

The nodal precession frequency ν_{NP} of orbits inclined relative to the equatorial plane of a neutron star is dominated by the prograde gravitomagnetic ‘torque,’ with a large retrograde (for prograde orbits) contribution from the classical quadrupole torque. In the cases considered in this pa-

per, the latter torque can amount at small orbital radii from about 10% to up to about 50% of the magnitude of the gravitomagnetic torque. The spin-induced deformation (oblateness) of the neutron stars renders, therefore, the low-PN ν_{NP} far more adequate (for orbits of moderate eccentricity) than the values obtained from Kerr black holes with the same M and j . However, for orbits of very small size ($r_a \lesssim 8$), even the low-order PN expressions overestimate ν_{NP} by up to 30% in the case of $j \approx 0.2$, stiff EOS L models.

Very stiff equations of state (e.g., L) have an important effect on the high-frequency portion of the set of all available frequencies ν_K , ν_r of eccentric orbits: due to the large stellar equatorial radii, orbits with very low periastra do not exist. The consequent absence of low values of ν_r at $\nu_{K,\text{isco}}/2 \lesssim \nu_K < \nu_{K,\text{isco}}$, for given M and ν_s , restricts severely the available subset of the ν_K - ν_r plane. For this reason, very stiff equations of state do not permit successful modeling of the neutron-star LMXBs’ kHz QPO frequencies in terms of the frequencies of eccentric orbits (see Markovic & Lamb 2000).

Acknowledgements

The author is indebted to Sharon Morsink, Scott Hughes, Fred Lamb and Luca Zampieri for enlightening discussions of conceptual and technical issues and to Nikolaos Stergioulas for making his code available. He has also benefited from conversations with Norman Murray, Vijay Pandharipande and Geoffrey Ravenhall. The Aspen Institute for Physics has provided a pleasant environment for interaction with colleagues. This work was supported in part by NSF grant AST 96-18524 and by NASA grant NAG 5-2925 at Illinois.

REFERENCES

- Akmal, A., Pandharipande, V. R. & Ravenhall, D. G. 1998, Phys. Rev. C, 58, 1804
- Arnett, W.D., Bowers, R.L. 1977, ApJ Suppl, 33, 415
- Arnol’d, V. A.. 1992, Ordinary Differential Equations. Springer, New York
- Bethe H.A. & Johnson, M.B. 1974, Nucl. Phys. A230, 1
- Chandrasekhar, S., 1983 The Mathematical theory of Black Holes. Oxford University Press, Oxford
- Cook, G.B., Shapiro, S.L. & Teukolsky, S.A. 1992, ApJ, 398, 203
- Cook, G.B., Shapiro, S.L. & Teukolsky, S.A. 1994a, ApJ, 422, 227
- Cook, G.B., Shapiro, S.L. & Teukolsky, S.A. 1994a, ApJ, 424, 823
- Hasinger, G. & van der Klis, M. 1989, A&A, 225, 79
- Hochstadt, H. 1975, Differential Equations: a Modern Approach. Dover Publications, New York
- Karas, V. 1999, astro-ph/9906425
- Komatsu, H., Eriguchi, Y. & Hachisu, I 1989, MNRAS 237, 355
- Komatsu, H., Eriguchi, Y. & Hachisu, I 1989, MNRAS 239, 153
- Laarakkers, W.G. & Poisson, E. 1997, ApJ 512, 282
- Marković, D. & Lamb, F.K. 2000, astro-ph/0009169, the companion paper.
- Miller, M. C., Lamb, F. K., & Psaltis, D. 1998, ApJ 508, 791
- Misner, C.W., Thorne, K.S. & Wheeler J.A., 1973, Gravitation. Freeman, San Francisco
- Morsink, S & Stella, L. 1999, ApJ 513, 827
- Nozawa, T., Stergioulas, N., Gourgoulhon, E. & Eriguchi, Y. 1989, A&A 132, 431
- Pandharipande, V. R., Akmal, A., & Ravenhall, D. G. 1998, in Nuclear Astrophysics, Proc. International Workshop XXVI on Gross Properties of Nuclei and Nuclear Excitations, ed.

- M. Buballa, N. Nörenberg J. Wambach, & A. Wirzba (Darmstadt: GSI), 11
- Pandharipande, V.R. & Smith, R.A. 1975, Phys. Lett 59B, 15
- Press, W.H., Teukolsky, S.A., Vetterling, W.T. & Flannery, B.P. 1992, Numerical Recipes (Cambridge University Press)
- Schiavilla, R., Pandharipande, V. R. & Wiringa, R. B. 1986, Nucl. Phys. A, 449, 219
- Stella, L. & Vietri, M. 1998, ApJ 492, L59
- Stella, L. & Vietri, M. 1999, Phys. Rev. Lett. 82, 17
- Stergioulas, N. & Friedman, J.L. 1995, ApJ 444, 306; Stergioulas' code is available on the ftp site alpha2.csd.uwm.edu, directory /pub/niksterg/rns
- Strohmayer, T. E., Zhang, W., Swank, J. H., Smale, A., Titarchuk, L., & Day, C. 1996, ApJ 469, L9
- van der Klis, M. 1998 in the Proceedings of the Third William Fairbank Meeting, Rome June 29 - July 4 1998, astro-ph/9812395
- van der Klis, M. 2000, Ann. Rev. Astr. & Astrophys., astro-ph/0001167
- van der Klis, M., Wijnands, R.A.D., Horne, K. & Chen W. 1997, ApJ, 481, L97
- Weinberg, S., 1972, Gravitation and Cosmology. Wiley, New York
- Wiringa, R.B., Fiks, V. & Fabrocini, A. 1988, Phys. Rev. C, 38, 1010